

CHCHD2 harboring the Parkinson's disease-linked T61I mutation precipitates inside mitochondria and induces precipitation of wild-type CHCHD2

Tom Cornelissen¹, Marco Spinazzi^{2,3}, Shaun Martin⁴, Peter Vangheluwe⁴, Bart De Strooper^{2,3},

Wim Vandenberghe^{1,5}

¹ Laboratory for Parkinson Research, Department of Neurosciences, KU Leuven, 3000 Leuven, Belgium

² VIB Center for Brain and Disease Research, 3000 Leuven, Belgium

³ Laboratory for the Research of Neurodegenerative Diseases, Department of Neurosciences, KU Leuven, 3000 Leuven, Belgium

⁴ Laboratory of Cellular Transport Systems, Department of Cellular and Molecular Medicine, KU Leuven, 3000 Leuven, Belgium

⁵ Department of Neurology, University Hospitals Leuven, 3000 Leuven, Belgium

Corresponding author: Prof. Wim Vandenberghe
Department of Neurology
University Hospitals Leuven
Herestraat 49
3000 Leuven
Belgium.
Tel. +32 16 344280
FAX +32 16 344285
E-Mail: wim.vandenberghe@uzleuven.be

ABSTRACT

The T61I mutation in CHCHD2, a protein residing in the mitochondrial intermembrane space, causes an autosomal dominant form of Parkinson's disease (PD), but the underlying pathogenic mechanisms are not well understood. Here, we compared the subcellular localization and solubility of wild-type and T61I mutant CHCHD2 in human cells. We found that mitochondrial targeting of both wild-type and T61I CHCHD2 depended on the four cysteine residues in the C-terminal coiled-coil-helix-coiled-coil-helix (CHCH) domain but not on the N-terminal predicted mitochondrial targeting sequence. The T61I mutation did not interfere with mitochondrial targeting of the mutant protein, but induced its precipitation in the IMS. Moreover, T61I CHCHD2 caused a reduction of complex IV activity and induced increased mitochondrial production of reactive oxygen species (ROS) and apoptosis, which was prevented by treatment with anti-oxidants. Retention of T61I CHCHD2 in the cytosol through mutation of the cysteine residues in the CHCH domain prevented its insolubilization as well as its apoptosis-inducing effect. Importantly, T61I CHCHD2 potently impaired the solubility of wild-type CHCHD2. In conclusion, our data show that the T61I mutation renders mutant CHCHD2 insoluble inside mitochondria, suggesting loss of function of the mutant protein. In addition, T61I CHCHD2 exerts a dominant-negative effect on the solubility of wild-type CHCHD2, explaining the dominant inheritance of this form of PD.

INTRODUCTION

Parkinson's disease (PD) is a common debilitating neurodegenerative disorder for which no disease-modifying treatment exists yet (1). Mitochondrial dysfunction plays a pivotal role in the pathogenesis of PD (2). Several genes linked to familial forms of PD, such as *PRKN*, *PINK1* and *LRRK2*, regulate mitochondrial function and mitochondrial quality control (3,4). Recently, mutations in *coiled-coil-helix-coiled-coil-helix domain containing 2* (*CHCHD2*), a nuclear gene encoding a small mitochondrial intermembrane space (IMS) protein, were linked to autosomal dominant PD (5). Evidence for pathogenicity is strongest for the T61I missense mutation, which was identified in three independent families with dominant PD (5,6). T61I is located in the central α -helix of CHCHD2 (5) (Fig. 1). CHCHD2 also contains an N-terminal predicted mitochondrial targeting sequence (MTS) and a C-terminal coiled-coil-helix-coiled-coil-helix (CHCH) domain characterized by a twin CX₉C motif containing four cysteine residues that form two disulfide bonds (5) (Fig. 1). Interestingly, mutations in the gene for CHCHD10, a close homologue of CHCHD2, cause amyotrophic lateral sclerosis/frontotemporal dementia (7).

Functional studies have shown that wild-type human CHCHD2 facilitates mitochondrial electron transport chain flux, probably via positive regulation of complex IV activity (8,9). Wild-type CHCHD2 has also been shown to inhibit apoptosis through interaction with BCL-xL and prevention of BAX oligomerization (10).

How *CHCHD2* mutations lead to PD, is not well understood. Previous studies in *Drosophila* were not conclusive, suggesting that *CHCHD2* mutations may cause PD via gain of function (11) or via loss of function and haploinsufficiency (12). In this study, we compared the subcellular localization and solubility of wild-type and T61I mutant CHCHD2 in human cells. We found that T61I mutation did not disrupt mitochondrial targeting of the mutant protein. However, T61I CHCHD2 became insoluble especially after entering mitochondria and, in

addition, strongly impaired the solubility of wild-type CHCHD2. These findings suggest that the T61I mutation is pathogenic via a combination of loss of function of the mutant protein and a dominant-negative effect on wild-type CHCHD2.

RESULTS

T61I mutation does not interfere with mitochondrial targeting of CHCHD2

To assess the effect of the T61I mutation on the subcellular localization of CHCHD2, we expressed human wild-type and T61I CHCHD2 (both with a C-terminal FLAG tag) in cultured primary human skin fibroblasts (Fig. 2). Transfection efficiency was 89.3 ± 2.5 % for wild-type CHCHD2 and 87.4 ± 3.1 % for T61I CHCHD2. Immunostaining (Fig. 2A) as well as western blot of cytosolic and mitochondrial fractions (Fig. 2B,C) revealed a similar, predominantly mitochondrial localization for wild-type and T61I CHCHD2, indicating that the T61I mutation did not interfere with mitochondrial targeting.

Mitochondrial targeting of CHCHD2 was previously reported to occur via the Mia40/Erv1 redox-coupled thiol-disulfide exchange system with an essential role for the four cysteine residues in the CHCH domain (9,13). By contrast, another study found that mitochondrial targeting of CHCHD2 depended on the MTS (5). We generated wild-type and T61I CHCHD2 constructs lacking the MTS (Δ MTS). Immunostaining and western blot of subcellular fractions showed that mitochondrial localization of Δ MTS wild-type and Δ MTS T61I CHCHD2 was similar to that of full-length wild-type and T61I CHCHD2 (Fig. 2A-C), indicating that the MTS was not required for mitochondrial targeting of CHCHD2. By contrast, when all four cysteine residues in the CHCH domain were replaced by serines, mitochondrial localization of wild-type and T61I CHCHD2 was largely abolished (Fig. 2A-C), consistent with Mia40/Erv1 pathway-mediated mitochondrial import of CHCHD2 (9).

T61I CHCHD2 is less soluble than wild-type CHCHD2

Next, we compared the solubility of wild-type and T61I FLAG-tagged CHCHD2 by performing sequential extractions on whole-cell lysates using buffers of increasing protein extraction strengths (Fig. 3A). Wild-type CHCHD2 was almost completely solubilized after extraction in high-salt buffer without detergent and high-salt buffer with 1 % Triton X-100. By contrast, a much smaller portion of T61I CHCHD2 was extracted in these mild extraction buffers, and most T61I CHCHD2 was found in the Triton X-100- and CHAPSO-resistant, SDS-extractable fraction, indicating a dramatic reduction in solubility compared with wild-type CHCHD2 (Fig. 3A). Similarly, untagged T61I CHCHD2 was much less soluble than untagged wild-type CHCHD2 (Supplementary Material, Fig. S1A).

T61I CHCHD2 precipitates in the IMS

To determine whether insoluble T61I CHCHD2 accumulated in the cytosol or in mitochondria, we performed serial extractions on cytosolic and mitochondrial fractions. Wild-type CHCHD2 was mostly Triton X-100-extractable, both in the cytosolic and mitochondrial fractions (Fig. 3B-D). T61I CHCHD2 was also mostly Triton X-100-extractable in the cytosol (Fig. 3B,D). By contrast, mitochondrial T61I CHCHD2 was almost completely found in the Triton X-100-resistant, SDS-extractable fraction (Fig. 3B,D), suggesting that T61I CHCHD2 became drastically less soluble in the mitochondrial fraction.

Next, we asked whether T61I CHCHD2 would still precipitate if it was prevented from entering the mitochondria. To retain T61I CHCHD2 in the cytosol, we replaced the four cysteine residues of the CHCH domain by serines, as described above (Fig. 2A,B). Interestingly, retention of T61I CHCHD2 in the cytosol prevented its precipitation (Fig. 3E,F), further

supporting the idea that T61I CHCHD2 becomes insoluble mainly after entering the mitochondria.

We then determined whether the insoluble T61I CHCHD2 in the mitochondrial fraction was associated with the outer mitochondrial membrane (OMM) (e.g. due to misfolding during mitochondrial import) or was present in the IMS. Isolated mitochondrial fractions were incubated with increasing concentrations of proteinase K, followed by extraction in SDS and western blot (Fig. 4). The proteinase K digestion pattern of both wild-type and T61I CHCHD2 closely resembled that of the IMS proteins HTRA2 and cytochrome c, and clearly differed from that of the OMM protein TOMM70 (Fig. 4). Taken together, the data suggested that insoluble T61I CHCHD2 was localized in the IMS.

T61I CHCHD2 does not trigger a mitochondrial unfolded protein response or mitophagy

Accumulation of misfolded proteins in the mitochondrial matrix can trigger the mitochondrial unfolded protein response (UPR^{mt}), an adaptive transcriptional program that promotes mitochondrial recovery (14). Prominent targets upregulated by the UPR^{mt} include mitochondrial matrix chaperones, such as HSP10 and HSP60, and the matrix protease CLPP (14). In addition, accumulation of misfolded proteins in the IMS was reported to induce a distinct form of UPR^{mt} that involves activation of the estrogen receptor and upregulation of the IMS protease HTRA2 and the mitochondrial regulator NRF1 (15). Levels of CLPP, HSP60, HTRA2 and NRF1 tended to be slightly higher in cells transfected with wild-type or T61I CHCHD2 than in cells transfected with empty vector, but did not differ between wild-type and T61I CHCHD2 (Fig. 5A,B), suggesting that mutant CHCHD2 did not induce a stronger UPR^{mt} than wild-type.

Mitochondrial damage can also induce mitophagy, a form of selective autophagy that removes dysfunctional mitochondria to prevent apoptosis (3). The PD-linked proteins PRKN and PINK1

are key mediators of mitophagy (3). To determine whether T61I CHCHD2 induced mitophagy, we performed mt-Keima imaging in cells transfected with wild-type and T61I CHCHD2 (4) (Fig. 5C,D). The mt-Keima probe is a fluorescent protein that is resistant to lysosomal proteases and exhibits pH-dependent excitation, allowing live dual-excitation ratiometric quantification of mitophagy (4,16). Basal mitophagy did not differ between cells expressing wild-type and T61I CHCHD2 (Fig. 5C-D). In conclusion, expression of T61I CHCHD2 failed to trigger the UPR^{mt} and mitophagy.

T61I CHCHD2 induces apoptosis via increased mitochondrial ROS production

CHCHD2 has been reported to affect the activity of the mitochondrial electron transport chain (8,9). To assess the effect of T61I CHCHD2 on mitochondrial respiration, we used high-resolution respirometry (17,18) (Fig. 6A,B). Fibroblasts transfected with wild-type or T61I CHCHD2 were suspended and treated with digitonin to permeabilize the plasma membrane while maintaining the integrity of the outer mitochondrial membrane. Oxygen consumption rates were measured after consecutive addition of a series of substrates and inhibitors of electron transport chain complex I, complex II and complex IV (Fig. 6A). Compared with wild-type, T61I CHCHD2 caused a non-significant trend towards reduced activity of complex I and complex II and a significant reduction of complex IV activity (Fig. 6A,B).

As defective function of complex IV is often associated with increased mitochondrial production of reactive oxygen species (ROS) (19), we measured mitochondrial ROS production using MitoSOX (4). Mitochondrial ROS production was indeed substantially higher in cells expressing T61I CHCHD2 compared with wild-type CHCHD2 (Fig. 6C).

Next, we used TUNEL assay and immunostaining for cleaved caspase 3 to assess the effect of wild-type and T61I FLAG-tagged CHCHD2 on cell survival. T61I CHCHD2 had a much stronger apoptosis-inducing effect than wild-type CHCHD2 (Fig. 6D-F). This was also true for

the untagged proteins (Supplementary material, Fig. S1B). Incubation with the ROS scavengers N-acetylcysteine or Mito-TEMPO prevented apoptosis induced by T61I CHCHD2 (Fig. 6G). Interestingly, retention of T61I CHCHD2 in the cytosol through mutation of the cysteine residues of the CHCH domain (Fig. 2A,B) abolished its apoptosis-inducing effect (Fig. 6H,I). Thus, T61I CHCHD2 only induced apoptosis when localized in mitochondria. Taken together, the data indicated that T61I CHCHD2 induced apoptosis via increased mitochondrial ROS production, likely as a result of a deleterious effect on electron transport chain activity.

Dominant-negative effect of T61I CHCHD2 on the solubility of wild-type CHCHD2

Finally, we asked whether T61I CHCHD2 had a dominant-negative effect on the solubility of its wild-type counterpart. We transfected cells with FLAG-tagged wild-type CHCHD2 in combination with either empty vector, untagged wild-type CHCHD2 or untagged T61I CHCHD2. Overexpression levels of untagged wild-type and untagged T61I CHCHD2 were similar (Fig. 7A). FLAG-tagged wild-type CHCHD2 was almost entirely present in the Triton X-100-extractable fraction when expressed alone or together with untagged wild-type CHCHD2, but became strikingly less soluble when coexpressed with untagged T61I CHCHD2 (Fig. 7A,B). Thus, T61I CHCHD2 potently impaired the solubility of wild-type CHCHD2.

DISCUSSION

Our findings show that the IMS protein CHCHD2 harboring the PD-causing T61I mutation becomes insoluble inside mitochondria, impairs the activity of respiratory complex IV and induces apoptosis via increased mitochondrial ROS production.

We show that T61I CHCHD2 overexpressed in primary human fibroblasts was dramatically less soluble than its wild-type counterpart. This is consistent with previous reports showing impaired solubility of T61I CHCHD2 relative to wild-type when expressed in HEK293 cells (20) or in *E. coli* (12). Importantly, reduced solubility of T61I CHCHD2 is unlikely to be an artifact of overexpression or ectopic expression, because a recent autopsy report demonstrated severely decreased solubility of endogenous CHCHD2 in the brain of a PD patient with the CHCHD2 T61I mutation (21). The T61I mutation substitutes a polar residue by a hydrophobic one, which could disturb proper folding of the protein and promote hydrophobic interactions. Remarkably, we found that solubility of T61I CHCHD2 was relatively preserved in the cytosol but drastically decreased in mitochondrial fractions, suggesting that T61I CHCHD2 becomes insoluble only after it enters the IMS. Several distinctive features of the IMS milieu may promote the tendency of T61I CHCHD2 to precipitate. The IMS is more acidic (22,23) and more oxidizing (24) than the cytosol. Moreover, very few chaperones are known to operate in the IMS. In contrast to almost all other cellular compartments, not a single member of the HSP40, HSP60 or HSP70 chaperone families has been identified in the IMS (25). Cells have evolved multiple mechanisms to protect themselves against the deleterious consequences of accumulation of misfolded proteins in mitochondria. One of these mechanisms is the UPR^{mt}, a response that transcriptionally upregulates mitochondrial chaperones and proteases to mitigate mitochondrial proteotoxicity (14). However, the UPR^{mt} is typically triggered by misfolded protein accumulation in the mitochondrial matrix and not the IMS, although one study reported the existence of a separate UPR^{mt} signaling pathway triggered by unfolded protein stress in the IMS (15). We observed no significant UPR^{mt} induction in response to T61I CHCHD2 expression in our experimental system. A more drastic line of defence against mitochondrial damage is mitophagy, a process that selectively removes dysfunctional mitochondria to prevent increased ROS production and apoptosis (3). The trigger

for mitophagy induction is disruption of mitochondrial import of PINK1, e.g. as a result of profound depolarization of the inner mitochondrial membrane or accumulation of misfolded proteins in the matrix (3). We did not find evidence of increased mitophagy in fibroblasts expressing T61I CHCHD2. Our data suggest that the failure of these cells to induce UPR^{mt} or mitophagy in response to T61I CHCHD2 resulted in continued presence of insoluble T61I CHCHD2 in the IMS, where it impaired complex IV activity, leading to increased ROS production and eventually apoptosis.

Insoluble CHCHD2 is very unlikely to be able to perform its physiological function. Thus, the insolubility of T61I CHCHD2 in the IMS points to a loss of function mechanism. Consistent with T61I being a loss of function mutation, previous work has shown that wild-type CHCHD2 suppressed an apoptotic phenotype in *CHCHD2* knockout mouse embryonic fibroblasts, while T61I CHCHD2 did not (12). Also, human wild-type, but not T61 mutant, CHCHD2 rescued mitochondrial defects, dopamine neuron loss and short life span in *Drosophila* deficient in the fly homologue of CHCHD2 (12). However, our data indicate that the pathogenic mechanism is more complex than pure loss of function of the mutant protein. We transfected wild-type and T61I CHCHD2 in fibroblasts expressing endogenous wild-type CHCHD2, and found that T61I CHCHD2 induced apoptosis when allowed to enter the IMS but not when it was retained in the cytosol, suggesting that mutant CHCHD2 exerts a toxic effect in the IMS. Consistent with a toxic effect of the mutant protein, overexpression of human T61I mutant CHCHD2 in *Drosophila* on a wild-type genetic background resulted in mitochondrial dysfunction, dopamine neuron loss and reduced life span (11). Importantly, we found that T61I CHCHD2 drastically impaired the solubility of wild-type CHCHD2. This potent dominant-negative effect of T61I CHCHD2 on the solubility of wild-type CHCHD2 and the associated likely loss of function of wild-type CHCHD2 can explain why the abnormalities we observed in wild-type cells overexpressing T61I CHCHD2 (impaired complex IV activity, increased mitochondrial ROS

production, increased apoptosis) closely resembled the phenotypes reported in CHCHD2-deficient cells (9,10). CHCHD2 is known to form homodimers (12,20). It is possible that wild-type, properly folded CHCHD2 still dimerizes with T61I mutant CHCHD2 and that the resultant dimer is less soluble, resulting in precipitation of the entire dimer. Alternatively, T61I mutant CHCHD2 may induce misfolding and precipitation of wild-type CHCHD2 in a prion-like fashion.

In conclusion, our data indicate that the T61I mutation renders mutant CHCHD2 insoluble in the IMS, implying loss of function of the mutant protein. In addition, the mutant protein exerts a dominant-negative effect on the solubility of wild-type CHCHD2, which can explain the dominant inheritance of this form of PD.

MATERIALS AND METHODS

Cell culture and transfection

Fibroblasts from healthy control subjects were obtained via skin biopsy from the medial aspect of the upper limb after written informed consent. All procedures were approved by the local ethics committee and were in accordance with the latest version of the World Medical Association Declaration of Helsinki. Fibroblasts were grown as described (4) in DMEM F12 (Invitrogen, 31331093) supplemented with fetal bovine serum (10%; Greiner Bio-One, 10270106), non-essential amino acids (1%; Thermo Fisher, 11140035), penicillin (100 U/ml; Thermo Fisher, 15140112), streptomycin (100 µg/ml; Thermo Fisher, 15140112) and sodium bicarbonate (0.12%; Sigma, S8761) at 37°C in a 5% CO₂ humidified atmosphere. Cultures were repeatedly tested for Mycoplasma infection and tests were always negative. Fibroblasts were transiently transfected using the Neon Transfection System (Invitrogen, MPK1096)

according to the manufacturer's instructions. Experiments were performed at passage numbers 5–15.

cDNA and antibodies

Vectors containing cDNAs for FLAG-tagged and untagged human CHCHD2 were purchased from Origene (RC209806, SC114478). The mt-Keima construct (mt/mKeima/pIND[SP1]) was a gift from Dr. A. Miyawaki (RIKEN Brain Science Institute, Japan) (16). The T61I mutation and the 4 cysteine to serine mutations were inserted with the Quikchange Lightning Site-Directed Mutagenesis kit (Agilent, 210518) using the following primers: T61I: 5'-GCCAGCTGCAGTGATTGCCATCTGGGCC-3' and 5'-GGCCCAGATGGCAATCACTGCAGCTGGC-3'; C114S: 5'-CTCATAGAGGCTAGGCTGCTGCTGCTGTGC-3' and 5'-GCACAGCAGCAGCAGCCTAGCCTCTATGAG-3'; C124S: 5'-CCCTGGTTCTGGGCACTCTCCAGAACTGTTTG-3' and 5'-CAAACAGTTTCTGGAGAGTGCCCAGAACCAGGG-3'; C134S: 5'-CTCATTGAAACCCTCACTGAGCTTGATGTCACCCT-3' and 5'-AGGGTGACATCAAGCTCAGTGAGGGTTTCAATGAG-3'; C144S: 5'-CGTTTGCAAGTCGGCTCTGTTTCAGCACCTC-3' and 5'-GAGGTGCTGAAACAGAGCCGACTTGCAAACG-3'. The Δ MTS construct was generated by PCR using primers: 5'-GCGATCGCCATGGGTCTGATGGCCCAGATGGC-3' and 5'-TCGAGCGGCCGCGTACGCGTGGC-3' on the FLAG-tagged CHCHD2 construct and cloned in the same backbone. All plasmids were verified by sequencing. The following primary antibodies were used for immunofluorescence (IF) or western blot (WB): mouse anti-FLAG (WB, 1:5000; IF, 1:1000; Sigma, F3165), rabbit anti-FLAG (WB, 1:1000; Sigma, F7425), mouse anti-ACTB (WB, 1:5000; Sigma, A5441), rabbit anti-HSP60 (IF, 1:1000; WB, 1:1000;

Abcam, ab53109), mouse anti-HTRA2 (WB, 1:1000; Antibodies Online, ABIN1107619), rabbit anti-cytochrome c (WB, 1:1000; GeneTex, GTX108585), mouse anti-TOMM70 (WB, 1:1000; Abnova, H00009868B01P), rabbit anti-CHCHD2 (WB, 1:500; ThermoFisher, PA5-23564), rabbit anti-NRF1 (WB, 1:1000; Abcam, ab175932), rabbit anti-CLPP (WB, 1:1000; Invitrogen, PA5-52722), rabbit anti-cleaved caspase 3 (IF, 1:200; Cell Signaling, 9661S). Peroxidase-linked secondary antibodies for WB were from GE Healthcare (NA931, NA934). Secondary antibodies for IF were donkey anti-mouse and anti-rabbit Alexa Fluor-488 and -555 (Thermo Fisher, a21202, a31570, a21206, a31572).

Immunofluorescence, TUNEL assay, confocal microscopy and image analysis

Immunostaining of cultured cells was performed as described previously (4,26). TUNEL assay was performed using the In Situ Cell Death Detection Kit, Fluorescein (Roche) according to the manufacturer's instructions. N-acetylcysteine and Mito-TEMPO were from Sigma. Confocal images with 1 μ m slice thickness were acquired at room temperature using a Leica TCS SP5 II confocal microscope equipped with a 63x objective lens (HC PL APO 63x/1.4 CS2), a multi-argon laser (458, 476, 488 nm), a He/Ne 543 nm laser and a HeNe 633 nm laser. Brightness and contrast were adjusted with NIH ImageJ software. Random images of at least 100 cells per condition were captured and analyzed by an investigator blinded to experimental conditions.

SDS-PAGE and western blot

Western blot was performed as described (4). In brief, fibroblasts were washed with ice-cold PBS, removed with a scraper and resuspended in PBS with 1% Triton X-100 (Sigma). After solubilization on ice for 30 min, insoluble material was removed by centrifugation at 20000 g for 5 min. Protein concentrations were determined using Bio-Rad Protein assay. SDS loading

dye was added to the samples, followed by denaturation at 99°C for 10 min, SDS-PAGE, blotting onto PVDF membranes and incubation with blocking solution, primary and secondary antibodies. Immunoreaction was visualized with ECL (Sigma, WBLUC, WBLUR) or ECL Prime (GE Healthcare, RPN2232) on a Fujifilm LAS-3000 Imager. The density of scanned signals was measured with UN-SCAN-IT gel 6.1 (Silk Scientific).

For sequential protein extraction from whole-cell lysates, fibroblasts were resuspended and incubated in high-salt buffer (50 mM Tris, 2 mM EDTA, 750 mM NaCl, pH 7.5) without any detergent for 30 min on ice and then centrifuged for 20 min at 20000 g at 4 °C. The supernatant (the high-salt-soluble fraction) was removed. The pellet was washed with high-salt buffer, incubated with high-salt buffer supplemented with 1 % Triton X-100 for 30 min on ice and centrifuged for 20 min at 20000 g at 4 °C. After removal of the supernatant (the Triton X-100-soluble fraction), the pellet was washed with high-salt buffer containing 1 % Triton X-100, incubated in high-salt buffer supplemented with 2 % CHAPSO for 30 min on ice and centrifuged for 20 min at 20000 g at 4 °C. After removal of the supernatant (the CHAPSO-soluble fraction), the pellet was washed with high-salt buffer containing 2 % CHAPSO, incubated in SDS buffer (50 mM Tris, 2 % SDS, pH 7,6) for 30 min and centrifuged for 20 min at 20000 g at room temperature. The supernatant was the SDS-soluble fraction. SDS loading dye was added to the samples, followed by heating at 99°C for 10 min and SDS-PAGE. Protease inhibitors (Roche, cOmplete™, EDTA-free Protease Inhibitor Cocktail) were present in all the extraction buffers.

To obtain Triton X-100-soluble (S) and Triton X-100-insoluble, SDS-extractable (I) fractions, fibroblasts were resuspended and incubated in PBS with 1% Triton X-100 on ice for 30 min. The sample was centrifuged at 20000 g for 5 min at 4°C. After removal of the supernatant (the S fraction), the pellet was incubated in SDS buffer for 30 min and centrifuged for 20 min at

20000 g at room temperature. The supernatant was the I fraction. SDS loading dye was added to the S and I samples, followed by heating at 99°C for 10 min and SDS-PAGE.

Subcellular fractionation

Mitochondria were isolated as described (4,26). Cells were harvested with a scraper, washed in PBS and homogenized with a glass pestle in isolation medium (250 mM sucrose, 1 mM EDTA, and 10 mM Tris-MOPS, pH 7.4) without any detergent. Nuclei and undisrupted cells were removed by centrifugation (600 g) for 10 min at 4°C. The supernatant was centrifuged at 7000 g for 10 min at 4°C and the resulting supernatant (containing cytosol) was separated from the pellet. The pellet was resuspended in isolation medium and centrifuged at 7000 g for 10 min at 4°C. This step was repeated three times. The final pellet (enriched in mitochondria) and the cytosolic fraction were analyzed by SDS-PAGE and western blot, or were first subjected to sequential protein extraction prior to SDS-PAGE and western.

To obtain S and I fractions from the mitochondrial and cytosolic samples, Triton X-100 was added to the mitochondrial and cytosolic fractions to a final concentration of 1 %, followed by incubation on ice for 30 min. The sample was centrifuged at 20000 g for 10 min at 4°C. After removal of the supernatant (S fraction), the pellet was incubated in SDS buffer for 30 min and centrifuged for 20 min at 20000 g at room temperature. The supernatant was the I fraction. The samples were heated in SDS loading dye as described above, followed by SDS-PAGE.

For proteinase K digestion assay, 20 µg of mitochondrial protein was treated with 0, 0.2, 0.5, 1, 2, 10 or 20 µg/mL of proteinase K for 20 min on ice. The reaction was ended by addition of SDS loading dye followed by heating at 99°C for 10 min and SDS-PAGE.

Mt-Keima imaging

Mt-Keima transfected cells were imaged as previously (4) in two channels via two sequential excitations (458 nm, green; 543 nm, red) and using a 600 to 695 nm emission range. Images were captured and analyzed by an investigator blinded for experimental conditions. At least 10 cells per condition were imaged with 0.5 μm slice thickness. Ratio (543/458) images were created using the Ratio Plus plugin in ImageJ. High (543/458) ratio areas were segmented and quantified with the Analyze Particles plugin in ImageJ. The total mitochondrial area was quantified with the Analyze Particles plugin by calculating the area of the total emission at 543 nm excitation. The parameter (high [543/458] ratio area/total mitochondrial area) was used as an index of mitophagy, as described (4,16).

High-resolution respirometry

High resolution respiration was measured as previously (17,18). In brief, cells were suspended in Miro6 buffer (18) at 37 °C. When needed H_2O_2 was added to reoxygenate the chambers by catalase-mediated O_2 generation. Three million transfected fibroblasts were loaded into the Oroboros 2K oxygraph. Digitonin was titrated up to 15 $\mu\text{g}/\text{ml}$ to permeabilize the cell membrane resulting in maximal substrate access to mitochondria and maximal complex I phosphorylating respiration. Oxygen consumption rates were measured before and after addition of the following sequence of substrates and specific inhibitors: 1) 2.5 mM pyruvate, 10 mM glutamate, and 1 mM malate to measure complex I-driven leak respiration; 2) 2.5 mM ADP to determine complex I-driven phosphorylating respiration; 3) 5 mM succinate to determine the phosphorylating respiration driven by simultaneous activation of complex I and II; 4) titrating concentrations of the mitochondrial uncoupler CCCP to reach the maximal uncoupled respiration (CI+II electron transfer capacity); 5) 200 nM rotenone to fully inhibit complex I-driven respiration and measure complex II-driven uncoupled respiration (CII electron transfer capacity); 6) 0.5 μM antimycin A to block mitochondrial respiration at the

level of complex III. Residual oxygen consumption was always negligible; 7) 2 mM ascorbate, 0.5 mM TMPD to measure complex IV-driven respiration; 8) 125 µg/ml cytochrome c to evaluate mitochondrial outer membrane integrity 9) 500 µM potassium cyanide (KCN) to specifically block complex IV activity and measure residual background oxygen consumption caused by chemical reaction between ascorbate and TMPD.

Measurement of mitochondrial ROS production

Mitochondrial ROS production was assessed using MitoSOX Red (Thermo Fisher, M36008) as described (4). Briefly, fibroblasts were transfected as indicated and plated in 12-well plates (at 100,000 cells per well) and allowed to attach overnight at 37°C. Cells were pulsed with MitoSOX (2 µg/ml) diluted in cell media for 30 min at 37°C. Subsequently, cells were rinsed twice with PBS, trypsinized and collected by centrifugation (300 x g, 5 min). Samples were then re-suspended in FACs buffer (PBS containing 1% BSA [Sigma, A7030], 2% fetal bovine serum) and kept on ice for the remainder of the experiment. The fluorescent intensities of 10,000 cells per condition were acquired using an Attune flow cytometer (Life Technologies).

Statistics

Significance of differences was analyzed with two-tailed Student's t-test for comparison between two groups and with one-way ANOVA and post hoc Holm – Sidak test for comparison between more than two groups (SigmaStat 3.5, Systat). Values and error bars represent mean ± SEM.

ACKNOWLEDGEMENTS

T.C. is a Postdoctoral Fellow and W.V. a Senior Clinical Investigator of the Research Foundation Flanders (FWO). This work was supported by KU Leuven (C12/17/008 and

'Opening the Future' campaign), FWO (Krediet aan Navorsers 1500817N) and the Queen Elisabeth Medical Foundation. We are grateful to A. Miyawaki for providing the mt-Keima construct.

CONFLICT OF INTEREST STATEMENT

The authors have no conflict of interest.

REFERENCES

1. Poewe, W., Seppi, K., Tanner, C.M., Halliday, G.M., Brundin, P., Volkman, J., Schrag, A.E. and Lang A.E. (2017) Parkinson disease. *Nat. Rev. Dis. Primers*, **3**, 17013.
2. Ryan, B.J., Hoek, S., Fon, E.A. and Wade-Martins R. (2015) Mitochondrial dysfunction and mitophagy in Parkinson's: from familial to sporadic disease. *Trends Biochem. Sci.*, **40**, 200-210.
3. Pickrell, A.M. and Youle, R.J. (2015) The roles of PINK1, parkin, and mitochondrial fidelity in Parkinson's disease. *Neuron*, **85**, 257-273.
4. Wauters, F., Cornelissen, T., Imberechts, D., Martin, S., Koentjoro, B., Sue, C., Vangheluwe, P. and Vandenberghe, W. (2019) LRRK2 mutations impair depolarization-induced mitophagy through inhibition of mitochondrial accumulation of RAB10. *Autophagy*, 10.1080/15548627.2019.1603548.
5. Funayama, M., Ohe, K., Amo, T., Furuya, N., Yamaguchi, J., Saiki, S. Li, Y., Ogaki, K., Ando, M., Yoshino, H., *et al.* (2015) CHCHD2 mutations in autosomal dominant late-onset Parkinson's disease: a genome-wide linkage and sequencing study. *Lancet Neurol.*, **14**, 274-282.

6. Shi, C.H., Mao, C.Y., Zhang, S.Y., Yang, J., Song, B., Wu, P., Zuo, C.T., Liu, Y.T., Ji, Y., Yang, Z.H., *et al.* (2016) CHCHD2 gene mutations in familial and sporadic Parkinson's disease. *Neurobiol. Aging*, **38**, 217.e9-217.e13.
7. Bannwarth, S., Ait-El-Mkadem, S., Chaussonot, A., Genin, E.C., Lacas-Gervais, S., Fragaki, K., Berg-Alonso, L., Kageyama, Y., Serre, V., Moore, D.G., *et al.* (2014) A mitochondrial origin for frontotemporal dementia and amyotrophic lateral sclerosis through CHCHD10 involvement. *Brain*, **137**, 2329-2345.
8. Baughman, J.M., Nilsson, R., Gohil, V.M., Arlow, D.H., Gauhar, Z., Mootha, V.K. (2009) A computational screen for regulators of oxidative phosphorylation implicates SLIRP in mitochondrial RNA homeostasis. *PloS Genet.*, **5**, e1000590.
9. Aras, S., Bai, M., Lee, I., Springett, R., Hüttemann, M., Grossman, L.I. (2015) MNRR1 (formerly CHCHD2) is a bi-organelle regulator of mitochondrial metabolism. *Mitochondrion*, **20**, 43-51.
10. Liu, Y., Clegg, H.V., Leslie, P.L., Di, J., Tollini, L.A., He, Y., Kim, T.-H., Jin, A., Graves, L.M., Zheng, J. *et al.* (2015) CHCHD2 inhibits apoptosis by interacting with Bcl-xL to regulate Bax activation. *Cell Death Differ.*, **22**, 1035-1046.
11. Tio, M., Wen, R., Lim, Y.L., Zukifli, Z.H.B., Xie, S., Ho, P., Zhou, Z., Koh, T.W., Zhao, Y. and Tan, E.K. (2017) Varied pathological and therapeutic response effects associated with CHCHD2 mutant and risk variants. *Hum. Mutat.* **38**, 978-987.
12. Meng, H., Yamashita, C., Shiba-Fukushima, K., Inoshita, T., Funayama, M., Sato, S. Hatta, T., Natsume, T., Umitsu, M, Takagi, J., *et al.* (2017) Loss of Parkinson's disease-associated protein CHCHD2 affects mitochondrial crista structure and destabilizes cytochrome c. *Nat. Commun.*, **8**, 15500.

13. Mesecke, N., Terziyska, N., Kozany, C., Baumann, F., Neupert W., Hell, K. and Herrmann, J.M. (2005) A disulfide relay system in the intermembrane space of mitochondria that mediates protein import. *Cell*, **121**, 1059-1069.
14. Pellegrino, M.W., Nargund, A.M. and Haynes C.M. (2013) Signaling the mitochondrial unfolded protein response. *Biochim. Biophys. Acta*, **1833**, 410-416.
15. Papa, L. and Germain, D. (2011) Estrogen receptor mediates a distinct mitochondrial unfolded protein response. *J. Cell Sci.*, **124**, 1396-1402.
16. Katayama, H., Kogure, T., Mizushima, N., Yoshimori, T., and Miyawaki, A. (2011). A sensitive and quantitative technique for detecting autophagic events based on lysosomal delivery. *Chem. Biol.*, **18**, 1042-1052.
17. Ye, F. and Hoppel, C.L. (2013) Measuring oxidative phosphorylation in human skin fibroblasts. *Anal. Biochem.*, **437**, 52-58.
18. Spinazzi, M., Radaelli, E., Horré, K., Arranz, A.M., Goukko, N.V., Agostinis, P., Maia, T., Impens, F., Morais, V.A., Lopez-Lluch, G., et al. (2019) PARL deficiency in mouse causes Complex III defects, coenzyme Q depletion, and Leigh-like syndrome. *Proc. Natl. Acad. Sci. U.S.A.*, **116**, 277-286.
19. Srinivasan, S. and Avadhani, N.G. (2012) Cytochrome c oxidase dysfunction in oxidative stress. *Free Radic. Biol. Med.*, **53**, 1252-1263.
20. Huang, X., Wu, B.P., Nguyen, D., Liu, Y.T., Marani, M., Hench, J., Bénit, P., Kozjak-Pavlovic, V., Rustin, P., Frank, S., Narendra, D.P. (2019) CHCHD2 accumulates in distressed mitochondria and facilitates oligomerization of CHCHD10. *Hum. Mol. Genet.*, **28**, 349.
21. Ikeda, A., Nishioka, K., Meng, H., Takanashi, M., Inoshita, T., Shiba-Fukushima, K., Li, Y., Yoshino, H., Mori, A., Okuzumi, A., et al. (2019) Mutations in CHCHD2 cause α -synuclein aggregation. *Hum. Mol. Genet.*, 10.1093/hmg/ddz241.

22. Cortese, J.D., Voglino, A.L. and Hackenbrock, C.R. (1992) The ionic strength of the intermembrane space of intact mitochondria is not affected by the pH or volume of the intermembrane space. *Biochim. Biophys. Acta*, **1100**, 189-197.
23. Porcelli, A.M., Ghelli, A., Zanna, C., Pinton, P., Rizzuto, R. and Rugolo M. (2005) pH difference across the outer mitochondrial membrane measured with a green fluorescent protein mutant. *Biochem. Biophys. Res. Commun.*, **326**, 799-804.
24. Hu, J., Dong, L. and Outten C.E. (2008) The redox environment in the mitochondrial intermembrane space is maintained separately from the cytosol and matrix. *J. Biol. Chem.*, **283**, 29126-29134.
25. Hermann, J.M. and Riemer, J. (2010) The intermembrane space of mitochondria. *Antioxid. Redox Signal.*, **13**, 1341-1358.
26. Cornelissen, T., Haddad, D., Wauters, F., Van Humbeeck, C., Mandemakers, W., Koentjoro, B., Sue, C., Gevaert, K., De Strooper, B., Verstreken, P., *et al.* (2014) The deubiquitinase USP15 antagonizes Parkin-mediated mitochondrial ubiquitination and mitophagy. *Hum. Mol. Genet.*, **23**, 5227-5242.

LEGENDS TO FIGURES

Figure 1. Schematic representation of CHCHD2 structure. Numbers indicate amino acid residues. The pathogenic T61I missense mutation is indicated in red. The four cysteine residues of the CHCH domain are indicated in black. MTS, mitochondrial targeting sequence. CHCH, coiled-coil-helix-coiled-coil-helix.

Figure 2. Mitochondrial targeting of CHCHD2 is not disrupted by the T61I mutation and depends on the CHCH domain. Human skin fibroblasts were transfected with full-length wild-type (WT) or T61I FLAG-CHCHD2, with WT or T61I FLAG-CHCHD2 lacking the mitochondrial targeting sequence (Δ MTS), or with WT or T61I FLAG-CHCHD2 in which all four cysteine residues of the CHCH domain were replaced by serines (4CS). **(A)** Cells were immunostained for FLAG and the mitochondrial marker HSP60, as indicated. Nuclei were visualized by TOTO-3 (blue). Scale bar, 10 μ m. **(B)** Mitochondrial (M) and cytosolic (C) fractions were isolated without any detergent, followed by SDS-PAGE and WB of C and M fractions. The same amount of total protein was loaded in each lane. The amount of CHCHD2 present in the C and M fractions was quantified as a percentage of total (C+M) CHCHD2 ($n \geq 3$ per condition).

Figure 3. T61I CHCHD2 is less soluble than wild-type CHCHD2. **(A)** Fibroblasts were transfected with wild-type (WT) or T61I FLAG-CHCHD2, followed by sequential protein extraction in high-salt buffer without detergent, Triton X-100 (1%), CHAPSO (2%) and SDS (2%), and analysis by SDS-PAGE and WB. **(B)** On the left, total cell lysates were subjected to sequential protein extraction in Triton X-100 (1%) and SDS (2%). Triton X-100-soluble (S) and Triton X-100-insoluble, SDS-extractable (I) fractions were analyzed with SDS-PAGE and WB. On the right, cytosolic (C) and mitochondrial (M) fractions were isolated without any

detergent from lysates of the same cells shown on the left, followed by sequential protein extraction in Triton X-100 and SDS. S and I fractions were analyzed with SDS-PAGE and WB. **(C,D)** Quantification of the data shown in (B). **(C)** The amount of S and I CHCHD2 relative to total (S+I) CHCHD2 was determined for WT and T61I ($n = 4$). * $P < 0.001$. **(D)** Quantification of the amount of S and I CHCHD2 relative to total (S+I) CHCHD2 present in the C and M fractions ($n = 4$). * $P < 0.05$ compared with the percentage of insoluble CHCHD2 in the T61 C fraction and the WT C and M fractions. **(E)** Fibroblasts were transfected with T61I CHCHD2 or T61I CHCHD2 in which the four cysteines of the CHCH domain were replaced by serines (4CS), followed by sequential extraction in Triton X-100 and SDS. S and I fractions were analyzed with SDS-PAGE and WB. **(F)** Quantification of the experiment shown in (D) ($n = 5$). * $P < 0.05$ compared with the percentage of T61I CHCHD2 in the I fraction.

Figure 4. Wild-type and T61I CHCHD2 are localized in the mitochondrial intermembrane space. Mitochondrial fractions were isolated without any detergent from fibroblasts transfected with wild-type (WT) or T61I CHCHD2, and were incubated with increasing concentrations (indicated above the blots in $\mu\text{g/ml}$) of proteinase K (PK), followed by extraction in SDS (PAGE and WB for FLAG, the outer mitochondrial membrane protein TOMM70 and the intermembrane space proteins HTRA2 and cytochrome c (Cyt. c).

Figure 5. T61I CHCHD2 does not trigger a substantial mitochondrial unfolded protein response or mitophagy. **(A, B)** Fibroblasts were transfected with empty vector (EV), wild-type (WT) or T61I CHCHD2. After 24 h, cell lysates were analyzed with SDS-PAGE and WB with the indicated antibodies. **(B)** Quantification of protein levels normalized to actin and EV ($n = 4$). **(C)** Fibroblasts were cotransfected with mt-Keima and either EV, WT or T61I CHCHD2, followed by live ratiometric mt-Keima imaging after 24 or 48 h. High (543:458)

signal corresponds to mito-Keima present in lysosomes. **(D)** High (543:458) ratio area divided by total mitochondrial area was quantified as an index of mitophagy ($n = 3$).

Figure 6. T61I CHCHD2 impairs complex IV activity and induces apoptosis via increased ROS production. **(A)** Representative illustration of high-resolution respirometry in fibroblasts transfected with wild-type (WT) or T61I CHCHD2. The blue trace indicates the O_2 concentration in **XXX cells**. The red (WT) and green (T61I) traces indicate the oxygen consumption rate. Three million cells were loaded in the oxygraph chamber in respiration buffer Miro6. Digitonin (Digi) was added to permeabilize the plasma membrane and make mitochondria accessible to substrates and ADP. Complex I (CI) substrates pyruvate/malate/glutamate (PMG) were added, followed by addition of a saturating concentration (2.5 mM) of ADP to measure CI-driven phosphorylating respiration (CI OxP). After addition of complex II (CII) substrate succinate (Succ), the phosphorylating respiration from both CI and CII was measured (CI+II OxP). Maximal uncoupled respiration, measured after progressive addition of the mitochondrial uncoupler CCCP, reflects the maximal electron transfer capacity from both CI and CII (CI+II ET). Addition of rotenone (Rot) blocks CI activity, resulting in CII-driven electron transfer capacity (CII ET). Antimycin A (Aa) completely blocks mitochondrial respiration at the level of complex III. Finally, complex IV (CIV)-driven electron transfer capacity (CIV ET) was measured as the cyanide (KCN)-sensitive respiration triggered by addition of the CIV substrates ascorbate (Asc) and TMPD. Exogenous cytochrome c (Cyt. c) was added to evaluate mitochondrial outer membrane integrity as a quality control procedure. H_2O_2 in the presence of catalase was added to reoxygenate the chamber. **(B)** Quantification of the respiratory states as measured in (A) ($n = 4$). * $P < 0.005$ compared with WT. As a loading control protein concentration was determined in the cells loaded in the chamber. Protein content of the WT CHCHD2- and T61I CHCHD2-transfected

cells was 0.92 ± 0.09 mg and 0.92 ± 0.95 mg, respectively ($n = 4$). **(C)** Fibroblasts were transfected with EV, WT or T61I CHCHD2 and mitochondrial reactive oxygen species were measured with mitoSOX (3.5 μ g/ml, 1 h) ($n = 4$). * $P < 0.001$ compared with EV and WT. **(D)** Fibroblasts were transfected with WT or T61I FLAG-CHCHD2. After 24 h apoptosis was detected using TUNEL staining. *Arrows* indicate TUNEL-positive cells. Nuclei were visualized by TOTO-3 (blue). Scale bar, 50 μ m. **(E)** The percentage of transfected cells that were TUNEL-positive was quantified. * $P < 0.001$ compared with WT CHCHD2 ($n = 3$). **(F)** 24 h after transfection with WT or T61I FLAG-CHCHD2 cells were immunostained for cleaved caspase 3 and FLAG. The percentage of transfected cells that were positive for cleaved caspase 3 was quantified ($n = 3$). * $P < 0.005$ compared with WT CHCHD2. **(G)** Fibroblasts were transfected with T61I FLAG-CHCHD2 and plated in medium with either DMSO, N-acetyl-cysteine (NAC, 5 mM) or Mito-TEMPO (10 μ M). After 24 h apoptosis in FLAG-positive cells was quantified using TUNEL stain ($n = 3$). * $P = 0.01$ compared with all other conditions. **(H, I)** Fibroblasts were transfected with WT or T61I FLAG-CHCHD2 or with WT and T61I FLAG-CHCHD2 in which the four cysteines of the CHCH domain were replaced by serines (4CS). After 24 h apoptosis in FLAG-positive cells was quantified with TUNEL assay or immunostaining for cleaved caspase 3. **(H)** Quantification of TUNEL staining ($n = 4$). * $P < 0.001$ compared with all other conditions. **(I)** Quantification of cleaved caspase 3 staining ($n = 3$). * $P < 0.05$ compared with all other conditions.

Figure 7. Dominant-negative effect of T61I CHCHD2 on solubility of wild-type CHCHD2.

(A) Fibroblasts were transfected with FLAG-tagged wild-type (WT) CHCHD2 in combination with either empty vector (EV), untagged WT CHCHD2 or untagged T61I CHCHD2. In the blots on the left, cell lysates were subjected to sequential protein extraction in Triton X-100 (1%) and SDS (2%). Triton X-100-soluble (S) and Triton X-100-insoluble, SDS-extractable (I)

fractions were analyzed with SDS-PAGE and WB. In the blots on the right, lysates from the same cells as on the left were boiled in SDS loading dye (without sequential extraction) and analyzed with SDS-PAGE and WB. *Arrowhead* and *asterisk* on the right of the CHCHD2 blot indicate the bands of transfected untagged CHCHD2 and FLAG-CHCHD2, respectively. **(B)** The amount of insoluble WT FLAG-CHCHD2 was quantified in the three cotransfection conditions (EV, untagged WT CHCHD2 and untagged T61I CHCHD2) ($n = 4$). * $P < 0.001$.

ABBREVIATIONS

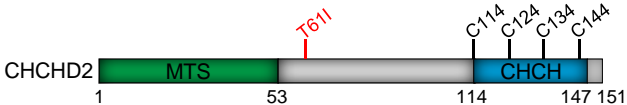


Figure 1

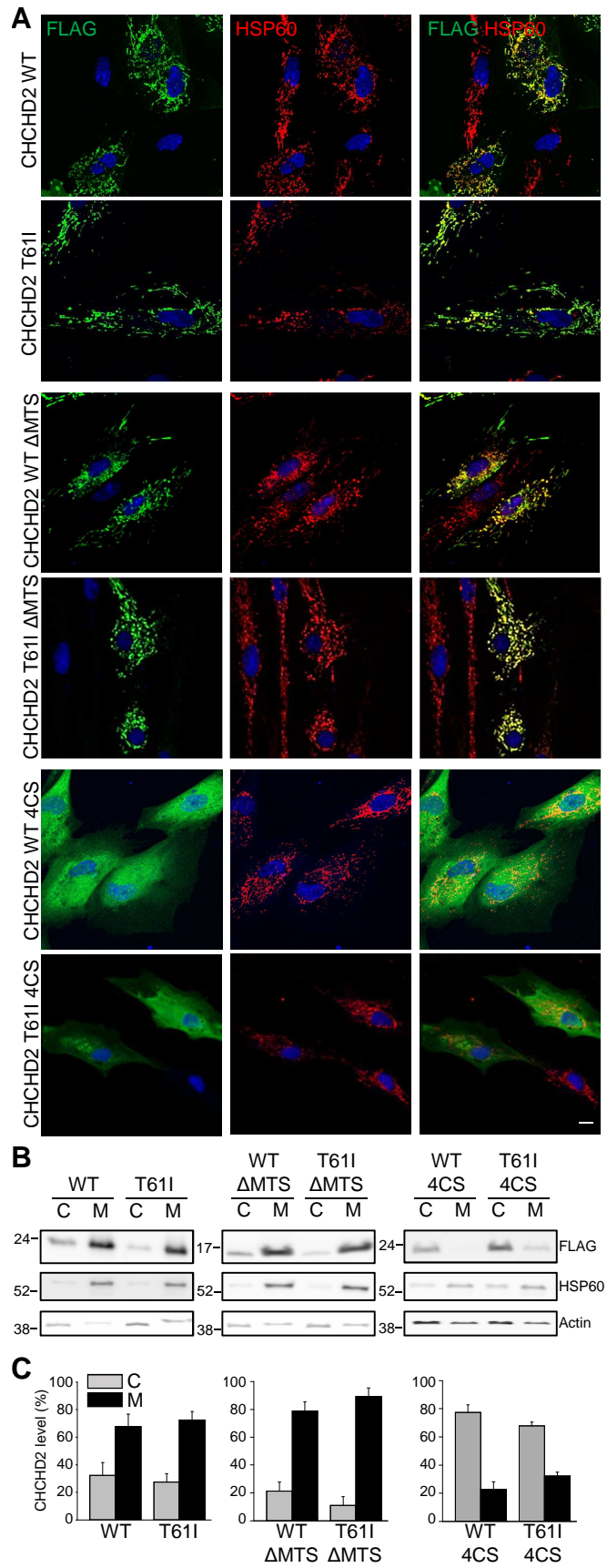


Figure 2

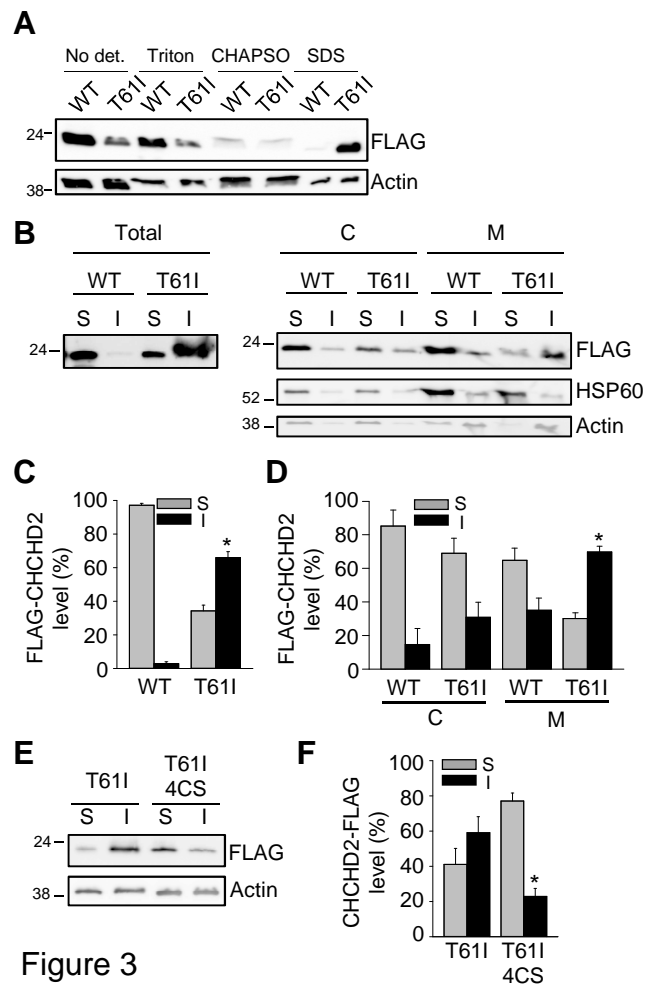


Figure 3

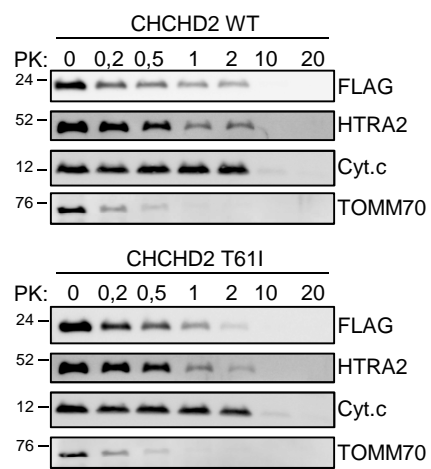


Figure 4

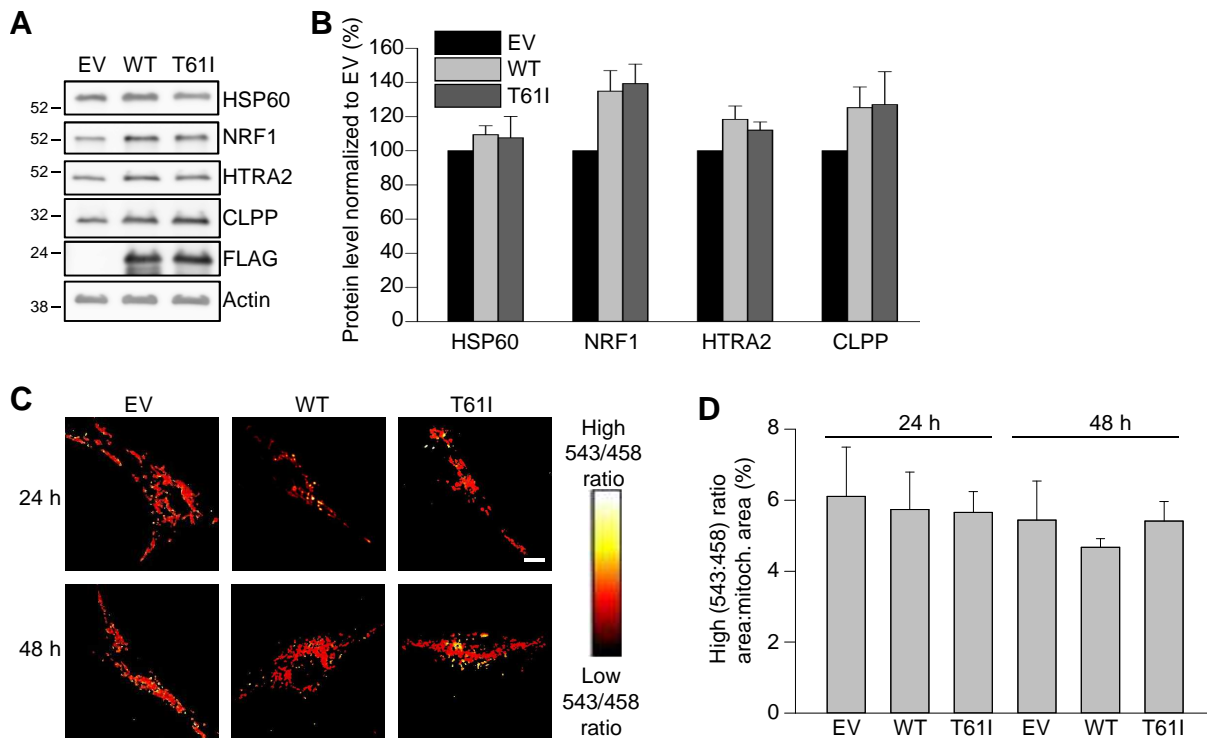


Figure 5

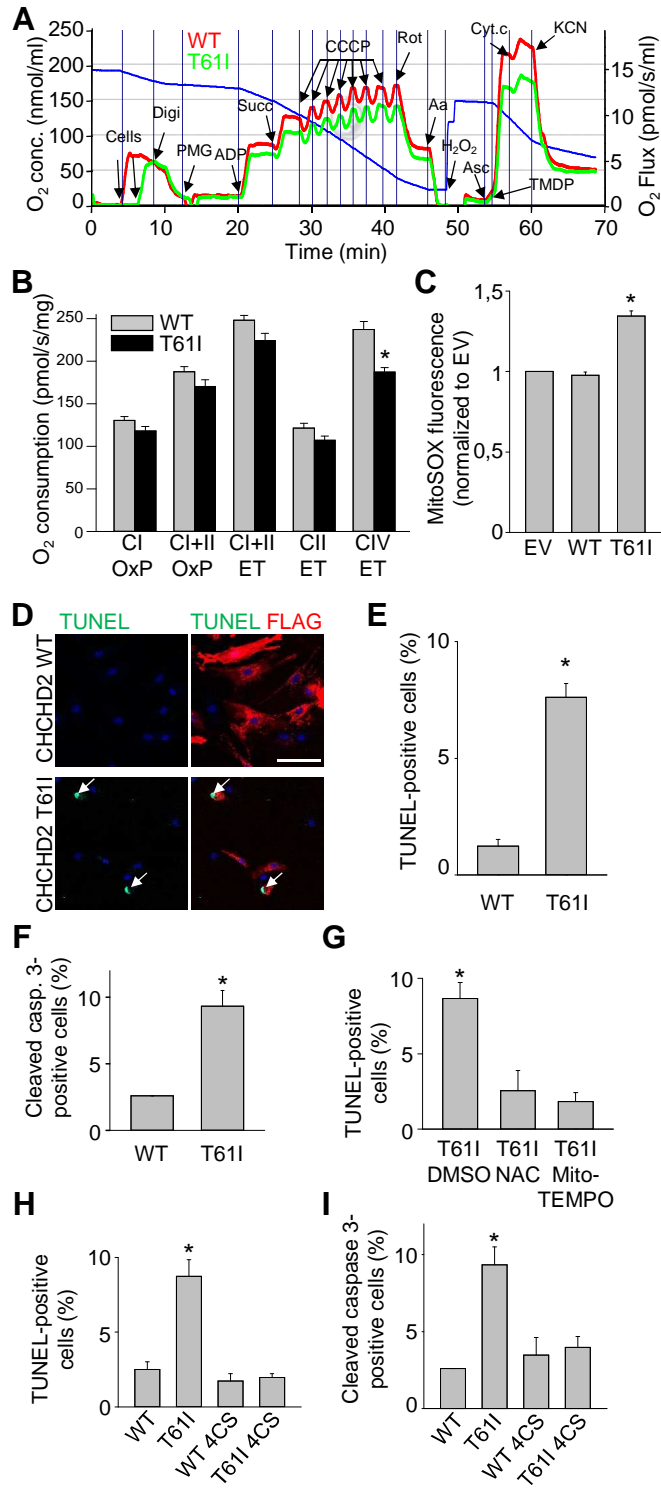


Figure 6

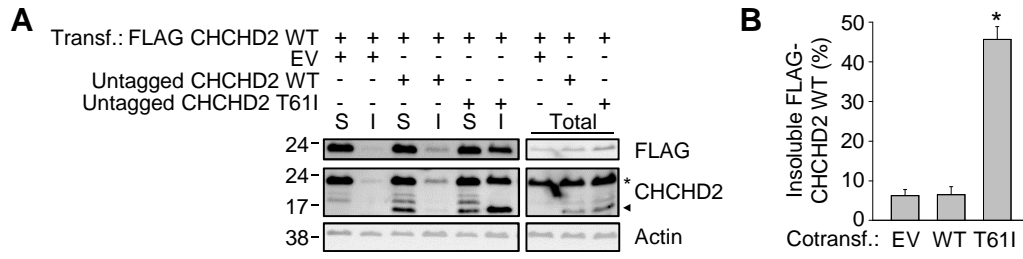
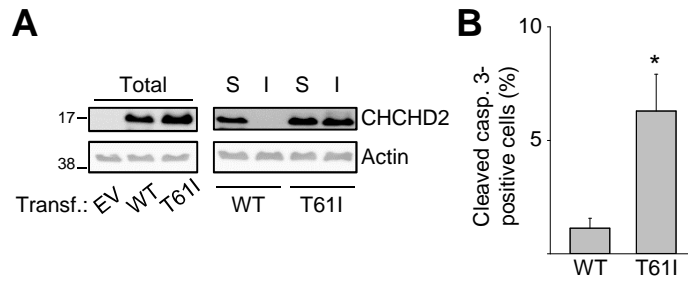


Figure 7



Suppl. figure S1. Untagged T61I CHCHD2 is less soluble than wild-type and induces apoptosis. (A) Fibroblasts were transfected with empty vector (EV), untagged wild-type (WT) or untagged T61I CHCHD2. In the blots on the right, cell lysates were subjected to sequential protein extraction in Triton X-100 (1%) and SDS (2%). Triton X-100-soluble (S) and Triton X-100-insoluble, SDS-extractable (I) fractions were analyzed with SDS-PAGE and WB. In the blots on the left, lysates from the same cells as on the right were boiled in SDS loading dye (without sequential extraction) and analyzed with SDS-PAGE and WB. **(B)** Fibroblasts were transfected with WT or T61I untagged CHCHD2. After 24 h cells were immunostained for cleaved caspase 3 and FLAG. The percentage of transfected cells that were positive for cleaved caspase 3 was quantified ($n = 3$). * $P < 0.05$ compared with WT.